Coordinated organization of mitochondrial lamellar cristae and gain of COX function during mitochondrial maturation in *Drosophila*

Yi-fan Jiang[a], Hsiang-ling Lin[b], Li-jie Wang[b], Tian Hsu[b], and Chi-yu Fu[b,*]
[a]Graduate Institute of Molecular and Comparative Pathobiology, School of Veterinary Medicine, National Taiwan University, Taipei 106, Taiwan; [b]Institute of Cellular and Organismic Biology, Academia Sinica, Taipei 115, Taiwan

ABSTRACT **Mitochondrial cristae contain electron transport chain complexes and are distinct from the inner boundary membrane (IBM). While many details regarding the regulation of mitochondrial structure are known, the relationship between cristae structure and function during organelle development is not fully described. Here, we used serial-section tomography to characterize the formation of lamellar cristae in immature mitochondria during a period of dramatic mitochondrial development that occurs after *Drosophila* emergence as an adult. We found that the formation of lamellar cristae was associated with the gain of cytochrome *c* oxidase (COX) function, and the COX subunit, COX4, was localized predominantly to organized lamellar cristae. Interestingly, 3D tomography showed some COX-positive lamellar cristae were not connected to IBM. We hypothesize that some lamellar cristae may be organized by a vesicle germination process in the matrix, in addition to invagination of IBM. OXA1 protein, which mediates membrane insertion of COX proteins, was also localized to cristae and reticular structures isolated in the matrix additional to the IBM, suggesting that it may participate in the formation of vesicle germination-derived cristae. Overall, our study elaborates on how cristae morphogenesis and functional maturation are intricately associated. Our data support the vesicle germination and membrane invagination models of cristae formation.**

Monitoring Editor
Thomas D. Fox
Cornell University

Received: Aug 16, 2019
Revised: Nov 13, 2019
Accepted: Nov 15, 2019

INTRODUCTION

Mitochondria are thought to have originated via endosymbiosis. As such, the organelles exhibit unique double-membrane architecture, consisting of outer and inner membranes that are separated by an intermembrane space. The inner membrane can be further subdivided into the inner boundary membrane (IBM) and the cristae invaginations based on ultrastructure, protein composition, and function (Mannella, 2006; Cogliati *et al.*, 2016). In the cristae, electron transport chain (ETC) complexes generate ATP by creating and maintaining a proton gradient between the matrix and the intermembrane space (Gilkerson *et al.*, 2003). Importantly, the morphology and remodeling of cristae are indicative of mitochondrial function, and the cristae ultrastructure is heavily influenced by several critical proteins (Scorrano *et al.*, 2002; Frezza *et al.*, 2006; Zick *et al.*, 2009; Cogliati *et al.*, 2013; Barbot and Meinecke, 2016; Quintana-Cabrera *et al.*, 2018). ATP synthase has been shown to play a structural role in cristae in addition to its enzymatic function, inducing positive membrane curvature at the cristae ridges (Strauss *et al.*, 2008; Davies *et al.*, 2011). Furthermore, the mitochondrial contact site and cristae organizing system (MICOS) complex is known to stabilize the cristae junction, the region where cristae connect to the IBM (Huynen *et al.*, 2016; Rampelt *et al.*, 2017; Schorr and van der Laan, 2018). Optic atrophy protein 1 (OPA1), a protein involved in inner membrane fusion, also plays a pivotal role in stabilizing cristae junctions and mediating cristae

This article was published online ahead of print in MBoC in Press (http://www.molbiolcell.org/cgi/doi/10.1091/mbc.E19-08-0450) on November 20, 2019.
The authors declare no competing financial interests.
Author contributions: C.-y.F. designed the experiments; Y.-f.J., H.-l.L., L.-j.W., and T.H. performed the experiments; C.-y.F. wrote the paper.
*Address correspondence to: Chi-yu Fu (fuchiyu@gate.sinica.edu.tw).
Abbreviations used: BSA, bovine serum albumin; COX, cytochrome *c* oxidase; cyt c, cytochrome *c*; DAB, 3,3′-diaminobenzidine; EM, electron microscopy; ETC, electron transport chain; IBM, inner boundary membrane; IFM, indirect flight muscle; MICOS, mitochondrial contact site and cristae organizing system; OM, outer membrane; OPA1, optic atrophy protein; PBS, phosphate-buffered saline; PDHA1, pyruvate dehydrogenase; SOD2, superoxide dismutase 2; TEM, transmission electron microscopy; WT, wild type.

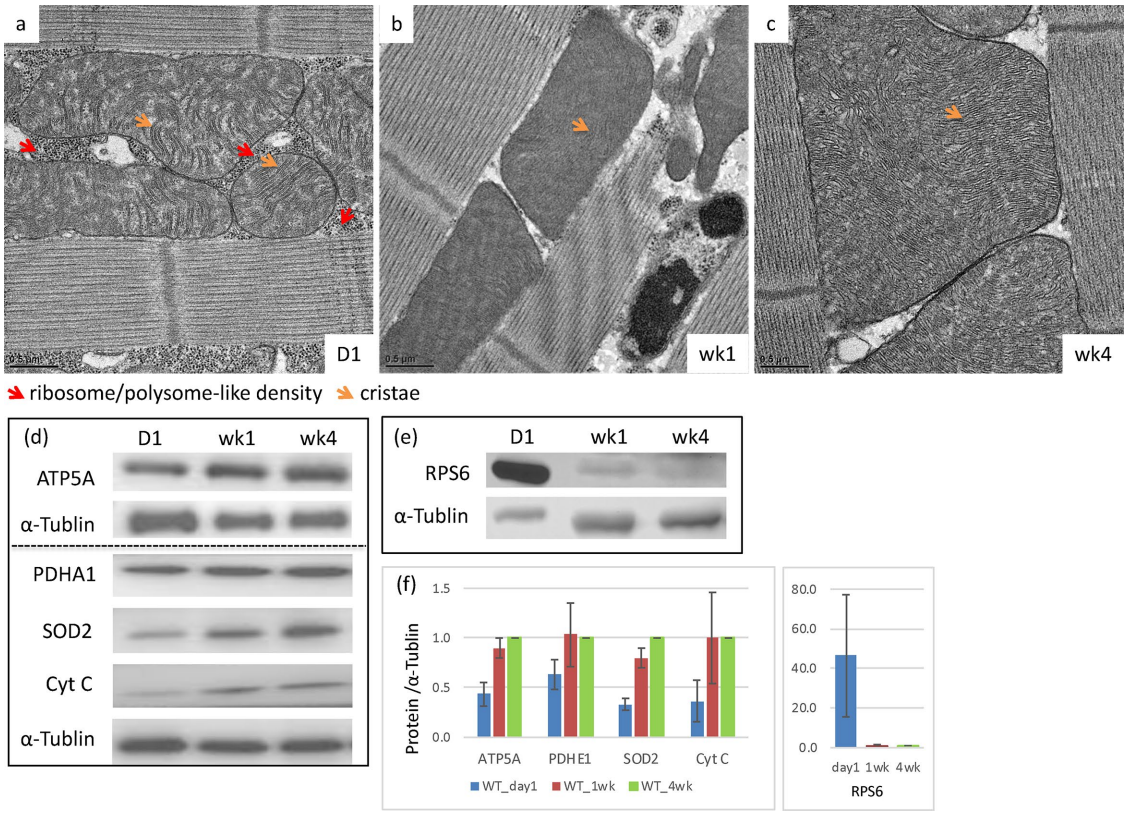

FIGURE 1: Mitochondria undergo development upon *Drosophila* eclosion. Thin-section EM micrographs of *Drosophila* IFM at day 1 (a), week 1 (b), and week 4 (c) showing the development of mitochondrial cristae. Red arrows indicate ribosome/polysomelike densities. Orange arrows indicate the cristae. Western blot analysis of mitochondrial proteins, ATP5A, PDHA1, SOD2, and CytC, and ribosomal protein, RPS6, in day 1, week 1, and week 4 flies (d, e). The relative protein abundance was quantified by densitometry and normalized to α-tubulin. The ratios were subsequently normalized to week 4 flies (f).

remodeling during apoptosis (Varanita *et al.*, 2015; MacVicar and Langer, 2016). Even though some key proteins have been identified as being essential for the maintenance and remodeling of cristae architecture, the process of functional cristae has not been characterized because the most common model systems do not exhibit distinct stages of cristae formation.

In this study, we examined the process of cristae formation during mitochondrial development in *Drosophila* after eclosion of adult flies from pupae. At the larval and pupal stages, *Drosophila* utilizes aerobic glycolysis to support the rapid accumulation of body mass and subsequent metamorphosis (Agrell, 1953; Tennessen *et al.*, 2011). At these stages, the mitochondria in the indirect flight muscle (IFM) scarcely contain lamellar cristae. Beginning at eclosion, mitochondria undergo rapid remodeling in the IFM, establishing densely arranged lamellar cristae that form connective membrane networks (Jiang *et al.*, 2017b). Thus, this physiological time window is highly useful to study the formation of functional cristae in immature mitochondria. Using this model system, we uncovered several novel aspects of the intricate association between cristae membrane morphogenesis and the acquisition of functionality during mitochondrial development.

RESULTS

Mitochondria undergo development upon *Drosophila* eclosion

We investigated mitochondrial morphogenesis and development in *Drosophila*, sampling the IFM of adult flies at various time points after eclosion. The global organization of IFM tissue was already established when adults emerged, with mitochondria distributed between parallel muscle fibers. Thin-section transmission electron microscopy (TEM) analysis showed that the mitochondria at day 1 after eclosion contained only a few organized cristae, which were loosely scattered throughout the matrix (Figure 1a). The mitochondria then developed densely packed lamellar cristae, usually within 1–2 d, becoming morphologically similar to those observed in older flies (Figure 1, b and c) (Jiang *et al.*, 2017b). The electron microscopy (EM) images also showed highly abundant ribosome- or polyribosomelike structures in the cytoplasm of the day 1 flies, which were not easily identified in week 1 or week 4 flies (Figure 1, a–c).

The expression levels of some mitochondrial proteins increased slightly as the flies aged from day 1 to week 4 after eclosion. Western blotting showed that several nuclear DNA-encoded mitochondrial proteins, including ATP5A (a subunit of ETC complex V), pyruvate dehydrogenase (PDHA1), superoxide dismutase 2 (SOD2), and cytochrome *c* (cyt c), were ~30–60% of week 4 levels in the day 1 flies (Figure 1, d and f). On the other hand, the level of ribosomal protein detected by anti-RPS6 was roughly 18-fold higher in day 1 flies compared with week 4 flies (Figure 1, e and f). This finding agrees with our observation of ribosome- or polyribosomelike densities in the EM micrographs of day 1 flies (Figure 1, a–c).

In a previous study, we characterized the 3D ultrastructure of mature mitochondria in *Drosophila* IFM, detailing the interconnected membrane networks formed by densely arranged lamellar cristae (Jiang *et al.*, 2017b). To characterize the 3D ultrastructure of

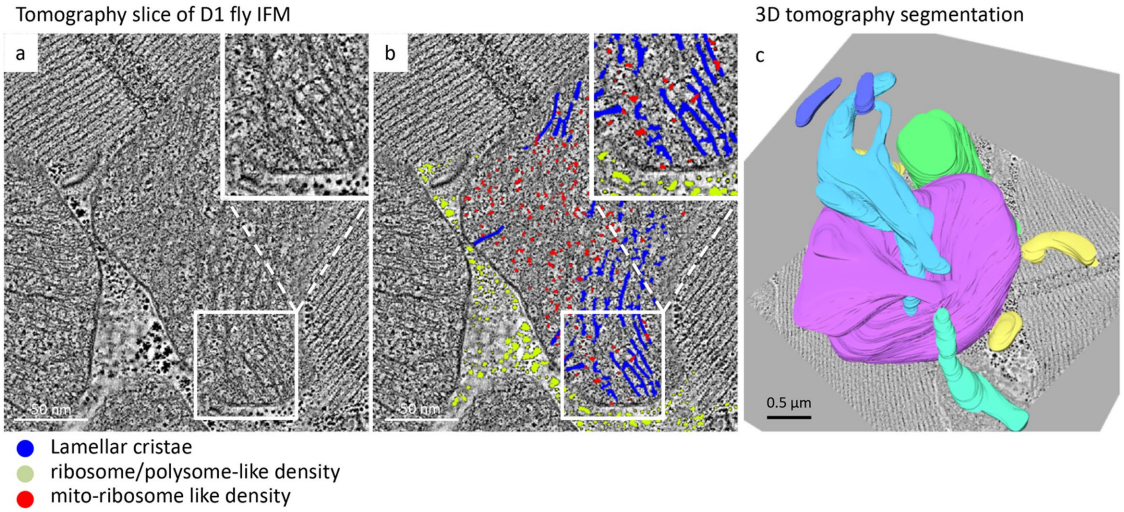

FIGURE 2: Serial-section tomography of immature mitochondria reveals cristae organization. Serial-section tomography slice (a) and segmentation (b) of *Drosophila* IFM at day 1. A few organized lamellar cristae are labeled in blue, cytoplasmic ribosomallike densities are green, and mitochondrial ribosomallike densities are red. (c) 3D segmentation of arbitrarily colored mitochondria showing the polymorphic shapes of immature mitochondria rather than the consistent ovoid shape of mature mitochondria.

immature mitochondria, we again used serial section electron tomography to reconstruct entire mitochondrial volumes. Mitochondria in the day 1 flies appeared relatively polymorphic with lamellipodialike or filopodialike extensions but matured to become ovoid-shaped and fill the cytoplasmic space between the muscle fibers (Figure 2c; Supplemental Movie S1). Only a few lamellar cristae were observed in the day 1 mitochondria with cytoplasmic ribosome- or polyribosomelike densities (Figure 2, a and b). A cryo-tomography study previously showed that cytoplasmic ribosomes associate with the mitochondrial surface via interactions with the TOM complex (Gold *et al.*, 2017). The tomograms of the day 1 flies also showed that the mitochondrial matrix contained numerous darkly stained ribosomelike molecules along with lamellar cristae (Figure 2, a and b). Mitochondrial translation machinery and its association with the inner membrane were previously described in great molecular detail using cryo-tomography on isolated yeast mitochondria (Pfeffer *et al.*, 2015). In the mature mitochondria, mitochondrial ribosomes could not be readily identified in the densely confined matrix compartment. Owing to a lack of available antibodies against the *Drosophila* mitochondrial ribosome, the levels of mitochondrial ribosome protein during maturation were not quantified. Taken together, our data clearly showed that after eclosion of adult *Drosophila*, IFM mitochondria underwent a dramatic maturation process to build lamellar cristae with high packing density.

Lamellar cristae formation in the immature mitochondria was coincidental with the gain of COX activity

The formation of functional cristae is likely to require proper coordination of membrane and protein assembly. To investigate how membrane morphogenesis is coupled with function, we took advantage of a classical method of Cyt *c* oxidase (COX) staining to visualize COX activity in the context of membrane ultrastructure (Seligman *et al.*, 1968). COX oxidizes 3,3′-diaminobenzidine (DAB) to form osmiophilic precipitates in the presence of osmium tetraoxide, which appears as dark staining under TEM. The osmium tetraoxide substrate also binds to the head group of phospholipids, creating weak contrast for lipid membranes.

The EM micrographs showed mature mitochondria at week 4 and were filled with lamellar cristae containing strong COX activity, which appeared darkly stained (Figure 3b). In the immature mitochondria of day 1 flies, positive COX activity was observed primarily in the organized lamellar cristae, while poorly organized structures were weakly stained and generally filled the matrix (Figure 3a).

To characterize the 3D arrangement of the COX-positive structures in immature mitochondria, serial section electron tomography was applied. Tomography of a whole-mitochondrion reconstruction is shown along the *z*-axis in Figure 4a. Positive COX signals were predominantly found in organized lamellae that were scattered throughout the

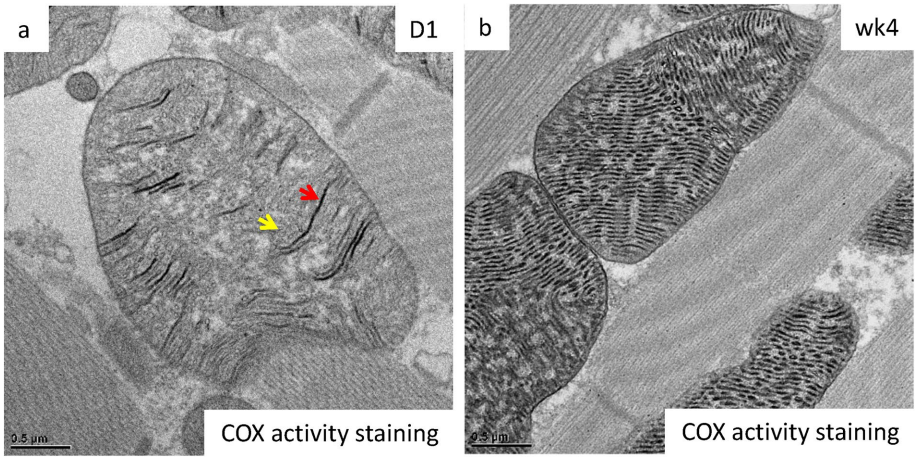

FIGURE 3: Lamellar cristae formation in immature mitochondria was coincident with the gain of COX activity. Thin-section EM micrographs of *Drosophila* IFM at day 1 (a) and week 4 (b) stained for COX activity.

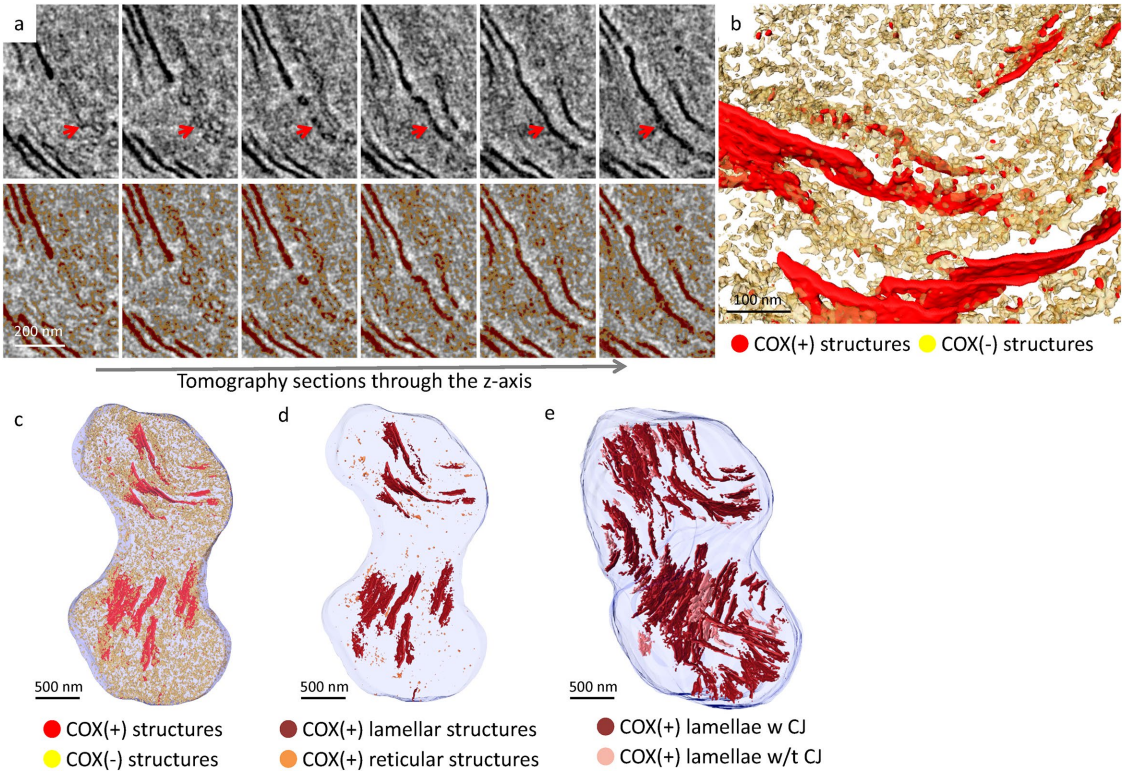

FIGURE 4: Cristae morphogenesis and functional maturation were associated during mitochondrial development. Serial-section tomography of *Drosophila* IFM at day 1 stained for COX activity. Tomography slices across the *z*-axis and the corresponding segmentation are shown in the top and bottom panels, respectively (a). At day 1, a few lamellar cristae show organization and strong COX staining, top panels. COX-positive structures are colored red and COX-negative structures are colored yellow in the bottom panels. The red arrows indicate a single lamellar crista across *z*-sections. 3D representations of the tomographic segmentation are shown in b and c to visualize the distribution of the COX-positive and COX-negative structures in a mitochondrion. (d) 3D representation of the tomographic segmentation showing COX-positive lamellar and reticular structures. (e) 3D representation of the segmentation of the whole serial-tomograms showing COX-positive lamellar cristae in or without connection to the IBM.

matrix (Figure 4a). The COX-negative structures appeared as poorly organized reticula in the 3D tomogram; thus, we refer to these structures as "reticular structures" (Figure 4a). Since these structures exhibit very limited COX activity, we do not describe them using the word "cristae." The 3D representations of COX-positive and COX-negative densities are shown in Figure 4, a–c. Analyzing the tomograms, the COX-positive and COX-negative volumes represented ~35 and 65% of the total densities, respectively (Table 1). Among the COX-positive densities, 69% appeared as organized lamellae, and 31% appeared as reticular structures that were defined by the volume larger or smaller than 1×10^6 nm^3, respectively (Table 1). Examples of COX-positive lamellar and reticular structures are shown in Figure 4d and Supplemental Figure S1, a and b. By careful visual inspection, no COX-negative densities were unambiguously identified as well-organized lamellar cristae.

Some physical loss of material between sections and missing-wedge effects from tomographic data collection occurred, leaving gaps and ambiguities in some regions of the joint tomograms (Lucic *et al.*, 2005). However, our analysis of regions with sufficient resolution clearly showed that some lamellar cristae did not connect to the IBM (Figure 4e; Supplemental Movie S2). Approximately 88% of lamellar cristae were connected to the IBM, while 12% were not (Figure 4e; Table 1). Cristae within 50 nm from the outer membrane (OM) or cristae in connection to other cristae in that definition were counted as being in contact with the IBM. Lamellar cristae in or without connection to the IBM are shown with color coding in Figure 4e and Supplemental Figure S1c. Because a portion of laminar cristae was not connected to the IBM, our observations are consistent with the idea that some lamellar cristae may be organized in the matrix by a process other than the invagination of the IBM.

COX4 in immature mitochondria localizes predominantly to organized lamellar cristae

To validate the COX activity-staining results, we generated a knock-in fly that expresses Apex2 conjugated to the C-terminus of endogenous COX4 gene, a subunit of COX that is synthesized in the cytoplasm and subsequently transported into the mitochondria (Supplemental Figure S2a). The heterozygous knock-in fly retains

Structures with COX activity	Positive 35%	Negative 65%
Morphology of COX(+) densities	Lamellar cristae 69%	Reticular structures 31%
Lamellar cristae	In contact with IBM 88%	Not in contact with IBM 12%

TABLE 1: Quantification of cristae structures in immature mitochondria.

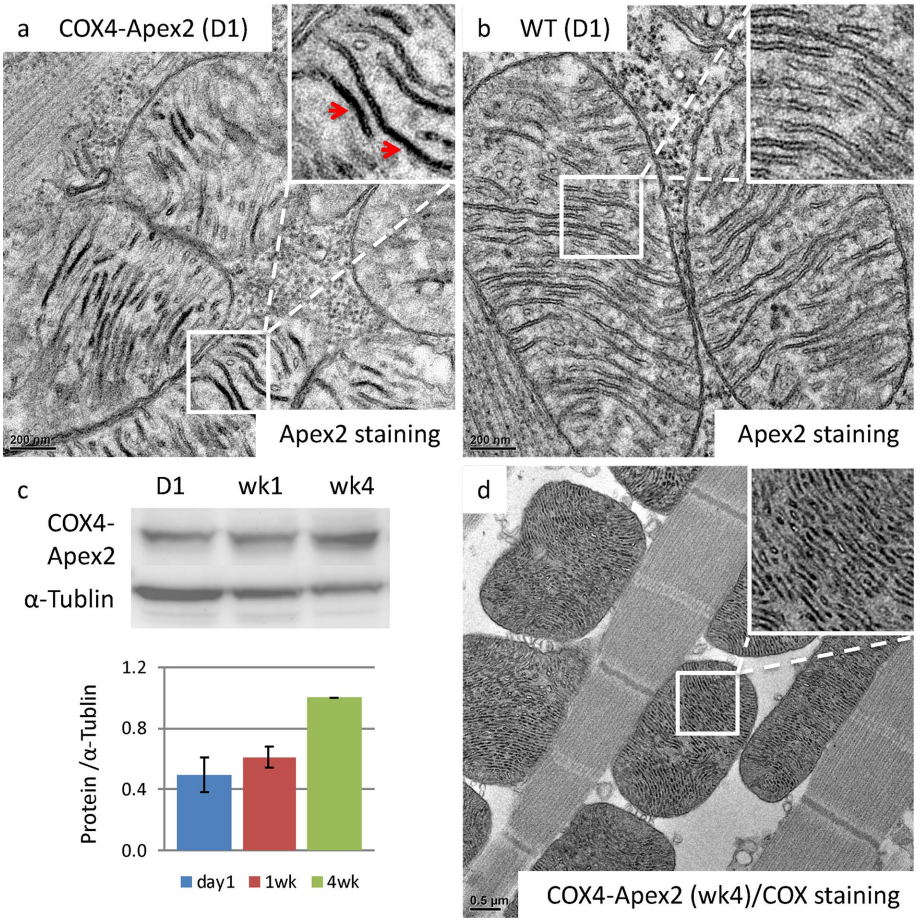

FIGURE 5: COX4 localizes predominantly to organized lamellar cristae. (a) Apex2 staining of the IFM of COX4-Apex2 knock-in flies at day 1. Positive Apex2 signals appeared darkly stained and were localized mainly in organized lamellar cristae. Red arrows indicate positive Apex2 staining in lamellar cristae. (b) Apex2 staining of WT flies at day 1 as a negative control. (c) The Western blot analysis of COX4-Apex2 expression at day 1, week 1, and week 4 by anti-flag tag. The relative protein abundance was quantified by densitometry and normalized to α-tubulin. The ratios were subsequently normalized to week 4 flies. (d) Thin-section EM of the IFM from COX4-Apex2 knock-in flies at week 4 stained for COX activity.

79% of wild-type (WT) COX activity (week 4) according to a standard colorimetric assay (Supplemental Figure S2b). Moreover, the COX activity and the expression of COX4-Apex2 in IFM increased slightly as the flies grew (Figure 5c; Supplemental Figure S2b). The mitochondria of COX4-Apex2 flies also showed positive EM staining for COX activities (Figure 5d). Apex2, an ascorbate peroxidase, catalyzes the polymerization of DAB in the presence of hydrogen peroxide (H_2O_2), which enhances EM contrast after osmium tetraoxide staining and allows the ultrastructural tracking of COX4 protein localization (Martell *et al.*, 2012). Using this method, COX4 was found to localize mainly in the organized lamellar cristae of immature mitochondria, which correlated with the COX activity staining data (Figure 5a). WT flies were used as a negative control for Apex2 staining (Figure 5b). According to structural data, the C-terminus of COX4 is apposed to the intermembrane space, which corresponds well with the Apex2 staining we observed in EM micrographs (Figure 5a; Supplemental Figure S2a) (Wu *et al.*, 2016). The correct localization of COX4-Apex2 indicated that the fusion protein was appropriately targeted to mitochondria. The proper folding and assembly of COX4-Apex2 fusion protein, as well as the COX colorimetric assay and EM staining, further indicated that the fusion protein does not substantially disrupt COX activity (Figure 5d; Supplemental Figure S2b).

OXA1 localization in immature mitochondria may support COX-positive cristae formation by a process other than the invagination of the IBM

Analysis of the tomograms showed that in immature mitochondria, a portion of COX-positive lamellar cristae was not connected to the IBM. These data agree with a vesicle germination model of cristae formation, wherein vesicles are formed either de novo in the matrix or by fission from existing cristae. Such vesicle-derived cristae would then later fuse with the IBM to establish cristae junctions (see Figure 7 later in this article).

For this hypothesis to hold, proteins for COX assembly should be observable in the cristae or reticular structures isolated from the IBM in immature mitochondria. The COX complex comprises multiple subunits encoded by both nuclear and mitochondrial DNA, and assembly of the COX complex requires OXA1-mediated insertion of both nuclear and mitochondrial DNA-encoded polypeptides from the matrix into the inner membrane (Bonnefoy *et al.*, 2009; Keil *et al.*, 2012; Soto *et al.*, 2012). Interestingly, the distribution of OXA1 in the cristae and IBM was previously shown to be dependent on the physiological condition of yeast cells (Stoldt *et al.*, 2012). Under nonrespiratory (fermentable) growth conditions, OXA1 is enriched in the IBM; conversely, OXA1 is enriched in the cristae under respiratory (nonfermentable) growth conditions.

We investigated the localization of OXA1 in the immature mitochondria using an OXA1-Apex2 knock-in fly. The flies were homozygous viable when the endogenous OXA1 gene was replaced by the OXA1-Apex2 transgene. The expression of OXA1-Apex2 fusion protein was confirmed by Western blot (Supplemental Figure S3a). Apex2 staining showed OXA1 was indeed present in the cristae and reticular structures isolated in the matrix additional to the IBM of immature mitochondria (Figure 6a). WT flies were used as a negative control for Apex2 staining (Figure 6b). Judging from the staining localization, the C-terminal Apex2 tag appeared to face the matrix side of the inner membrane; moreover, the staining appeared largely as granular densities (Figure 6a). The localization of the Apex2 tag on the matrix side was confirmed in S2 cells that overexpressed OXA1-Apex2 (Figure 6c). The high expression level of OXA1-Apex2 in S2 cells yielded very strong staining in the matrix. Mock-transfected cells served as negative controls for Apex2 staining (Figure 6d). A Western blot showing OXA1-Apex2 levels in the S2 cells is shown in Supplemental Figure S3b. In conclusion, our data showed that some OXA1 was localized to cristae and reticular structures isolated in the matrix additional to the IBM in immature mitochondria, which potentially can mediate COX-positive lamellar cristae formation in the matrix by a process other than the invagination of the IBM.

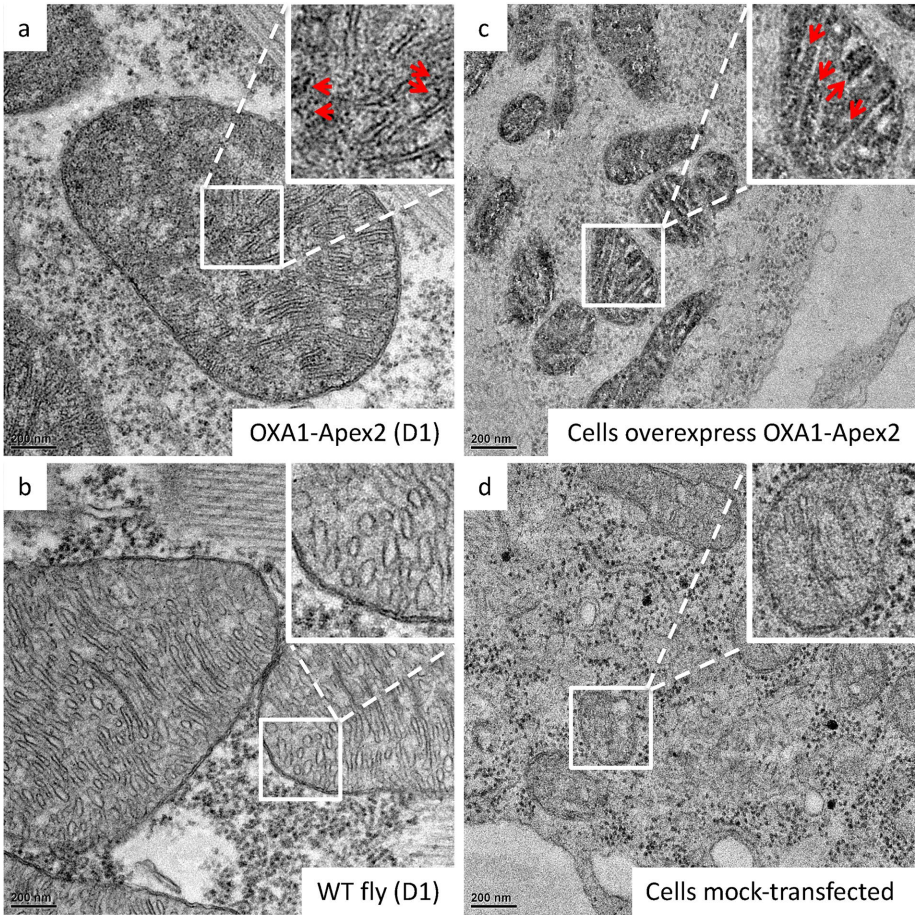

FIGURE 6: OXA1 localization in immature mitochondria supported COX-positive cristae formation by a process additional to the invagination of the IBM. Apex2 staining of the IFM of OXA1-Apex2 knock-in flies (a) and the WT control (b) at day 1. Positive OXA1-Apex2 staining appeared as granular densities on the matrix side of cristae and IBM where the Apex2 tag is expected to be localized. Apex2 staining of S2 cells transfected with (c) and without (d) plasmids expressing *D. melanogaster* OXA1-Apex2. High OXA1-Apex2 expression yielded strong staining on the matrix side of the cristae and IBM where the Apex2 tag is expected to be found. Red arrows in a and c indicate positive Apex2 staining on the matrix side of the membranes.

DISCUSSION

In this study, we tracked the dramatic mitochondrial development that occurs in IFM after eclosion of adult *Drosophila*. We showed that lamellar cristae formation in immature mitochondria was coincidental with the gain of COX activity. This finding was further supported by our observation that the COX4-Apex2 fusion protein was also primarily localized to the organized cristae lamellae of immature mitochondria. We observed that some COX-positive lamellar cristae were not in contact with the IBM in immature mitochondria. We, therefore, hypothesize that some lamellar cristae may form in the matrix by a process other than the invagination of the IBM. In line with this hypothesis, the OXA1 protein, which is known to mediate the membrane insertion of COX subunits, was present in cristae and reticular structures isolated in the matrix additional to the IBM. Overall, our study introduces previously unknown features of the intricately associated processes of cristae membrane morphogenesis and acquisition of functionality during mitochondrial development.

Through evolution, mitochondria have become delicately integrated into eukaryotic cells as organelles with highly functionalized compartments and membranes. Thus, it is no surprise that a sophisticated biomolecular interaction network regulates cristae architecture (Jayashankar *et al.*, 2016). One area of active investigation with regard to cristae architecture is the mechanisms of cristae formation. Previously, six theoretical models for the formation and maintenance of cristae were proposed (Zick *et al.*, 2009). These models can be grouped into three main categories: 1) the *invagination model*, where the cristae are formed through the invagination of the IBM; 2) the *fusion-mediated model*, where the cristae formation is associated with mitochondria fusion; and 3) the *vesicle germination model*, where vesicles that are either formed de novo in the matrix or by fission from existing cristae fuse with the IBM to establish cristae junctions and cristae. More recently, two other pathways for cristae formation have been proposed based on work in yeast. In one pathway, cristae are formed by the invagination of the IBM, independent of mitochondrial fusion, while in the second pathway, cristae formation involves mitochondrial fusion and OPA1-mediated inner membrane fusion (Harner *et al.*, 2016). This work provided an experimental foundation for the first two models previously discussed by Zick *et al.* (2009).

The data in our study do not rule out any of the three categorical models. Furthermore, our data support the existence of vesicle germination-derived cristae, where reticular structures (vesicles) in the matrix may organize into functional lamellar cristae. Therefore, we hypothesize that cristae are derived from some combination of the invagination and vesicle germination models, in addition to the fusion-mediated model. As such, lamellar cristae may 1) organize at the cristae junction and extend from the IBM as the membranes acquire COX function or 2) extend from the matrix sides by organizing the reticular structures in coordination with OXA1-mediated COX assembly. Lamellar cristae may also 3) form in the matrix as reticular structures, which later contact the IBM and establish MICOS-stabilized cristae junctions (Figure 7). Notably, it is unclear how COX and OXA1 might be transported to the matrix without the involvement of cristae junctions in the vesicle germination model. Thus, our hypothetical model requires further investigation and experimental elucidation.

The generalized mechanism of protein-coupled membrane morphogenesis is well documented in various membrane remodeling processes, such as vesicle budding and fusion (Bonifacino and Glick, 2004). Previously, ATP synthase has been demonstrated to play an essential role in cristae morphogenesis (Strauss *et al.*, 2008; Davies *et al.*, 2011), and cristae morphology reciprocally influences the ETC supercomplex assembly and respiratory efficiency (Cogliati *et al.*, 2013). The intimate connection of cristae morphology with ETC assembly and function is reiterated by our observations. COX complex assembly has been described in great detail and involves the coordination of multiple steps, including protein synthesis, membrane insertion, assembly, and metal incorporation, all of which are

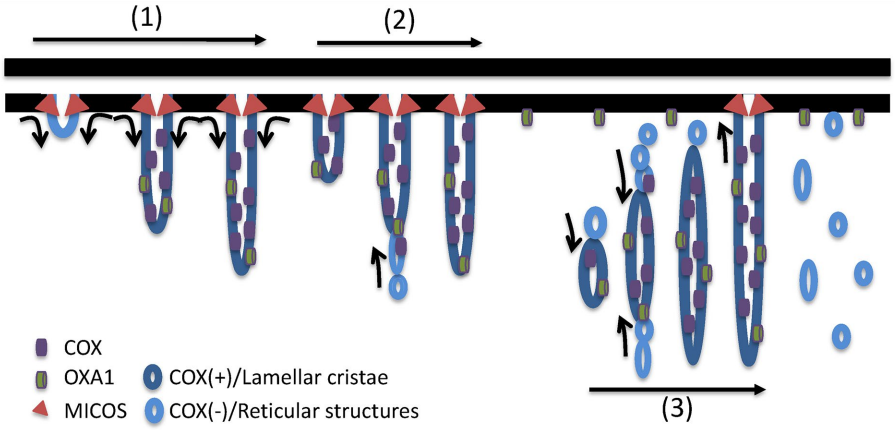

FIGURE 7: Hypothetical model of cristae formation. Lamellar cristae (1) organize at the cristae junction and extend from the IBM as the membranes acquire COX function, or (2) extend from the cristae from the matrix side by organizing reticular structures in coordination with OXA1-mediated COX assembly. (3) Lamellar cristae form in the matrix as organized reticular structures, which later contact the IBM and establish cristae junctions via MICOS.

mediated by various chaperones and accessory proteins (Soto *et al.*, 2012). Our study reveals an additional layer of coordination during COX assembly, which is an association with the establishment of cristae ultrastructure. Whether COX assembly directs the lamellar cristae formation or vice versa, or whether the two events are coordinated by a master regulator, remains to be further elucidated.

MATERIALS AND METHODS

Fly strains

Drosophila strains on the Oregon-R-P2 background (WT) were used in these studies. Apex2-Flag knock-in flies of COX4 and OXA1 were generated by CRISPR/Cas9-mediated genome editing and homology-dependent repair using guide RNA(s) and a double-stranded DNA plasmid donor. The PBac system was used to facilitate genetic screening (Well Genetics).

High-pressure freezing and freeze substitution (HPF/FS) specimen preparation for morphological observation

Flies were anesthetized on ice and embedded in 4% low melting agarose in 0.1 M phosphate buffer. Embedded flies were then sectioned to 100-μm-thick slices by a vibrating blade microtome (Leica VT1200S) and fixed in 2.5% glutaraldehyde in phosphate buffer. HPF/FS was performed as previously described (Jiang *et al.*, 2017a, b). The tissue sections were washed in three drops (~150 μl) of phosphate buffer, followed by two drops (~100 μl) of phosphate buffer with 20% bovine serum albumin (BSA). The specimens were subsequently placed in the gold carrier filled with 20% BSA in phosphate-buffered saline (PBS). The carriers were loaded into a high-pressure freezer (Leica EM HPM100) according to the manufacturer's instructions. The carriers were subsequently released from the holder under liquid nitrogen and transferred to the chamber of a freeze-substitution device (Leica EM AFS2) precooled to –140°C and incubated for 96 h. before FS.

During FS, the temperature of the chamber was raised to 0°C with a change of 5°C/h. During the process, the specimens were substituted with 0.1% uranyl acetate and 2% glutaraldehyde in acetone at –60°C for 12 h, followed by 2% osmium tetroxide at –25°C for 12 h, and washed with acetone at 0°C 3× for 1 h each. The specimens were subsequently removed from the carriers using a needle and infiltrated and embedded in EMBed-812 resin at room temperature, which was polymerized at 65°C for 16 h. The specimen blocks were trimmed and sectioned using an ultramicrotome. The sections were stained with Reynold's lead citrate for 10 min and subjected to TEM inspection.

Serial section electron tomography

The procedure was performed as previously described (Jiang *et al.*, 2017a,b). Serial sections with a thickness of 200 nm were prepared and collected on copper slot grids (2 × 0.5 mm oval slots) with carbon supports, which were overlaid with 10 nm fiducial gold that was pretreated with BSA. The grids were stained with Reynold's lead citrate before the second layer of fiducial gold was applied. The specimens were imaged with an FEI Tecnai TEM operating at 200 kV. The micrographs were recorded with a Gatan UltraScan 1000 CCD at 0.87 nm/pixel (9600×). Tilt series from –60° to +60° with 2° increments were acquired at 10 μm defocus using Leginon automatic data collection software (Suloway *et al.*, 2009). Double tilt series were collected using a double tilt holder (Model 2040 Dual-Axis Tomography Holder; Fischione). Serial tomograms were reconstructed, joined using IMOD, and segmented using Avizo 3D software (FEI).

EM staining for COX activity

The procedure was performed as previously described (Seligman *et al.*, 1968) with minor modifications. Vibrating blade microtome sections of fly tissues were washed with PBS and stained for 3 h at 37°C in a staining solution containing 5 mg DAB, 9 ml sodium phosphate buffer (0.05 M, pH 7.4), 750 mg sucrose, 20 μg catalase (dissolved in 0.05 M potassium phosphate buffer, pH 7.0), and 10 mg cyt c (dissolved in distilled water) at a volume of 10 ml. Subsequently, the specimens were washed with PBS for 1 h and subjected to standard osmium fixation, dehydration, infiltration, and embedding with Embed-812 resin. The blocks were cut to thin sections of 70 nm thickness and observed under TEM without further staining.

Image analysis of tomography stained for COX activity

The image analysis was carried out using Avizo 3D software (FEI). First, the mitochondrial OM of the tomographic reconstruction was defined manually. The COX-positive versus -negative densities within the OM were segmented automatically by a threshold method and the volumes of COX-positive versus -negative densities were calculated. The COX-positive lamellar versus reticular structures were defined by the volume larger or smaller than 1×10^6 nm^3, respectively. The cristae in contact with the IBM were defined by the cristae within the distance of 50 nm from the OM. By manual inspection, cristae connecting to the other cristae within the distance of 50 nm from the OM were also counted as being in contact with the IBM.

Apex2 staining EM

The protocol was modified from a previously described method (Hung *et al.*, 2016). Vibratome sections of the fly tissues were fixed in 2% glutaraldehyde in 0.1 M sodium cacodylate with 2 mM $CaCl_2$, pH 7. Residual glutaraldehyde was washed off with buffer (2 min, 5×) and quenched with 20 mM glycine followed by more washes (2 min, 5×). The specimens were subsequently stained with 0.5 mg/ml DAB-4HCl and 0.3% H_2O_2 in the buffer for 30 min, washed with buffer (10 min, 5×), and stained with 1% osmium

tetroxide for 30 min. After washing with ddH_2O (10 min, 3×), the specimens were stained with 1% uranyl acetate overnight. The specimens were further dehydrated and embedded in resin for thin-section and TEM observation.

Cell culture for Apex2 staining

S2 cells were seeded in a 6-well culture plate at 1×10^6 cells/ml and grown for another day to (2–4) $\times 10^6$ cells/ml. The cells were then transfected with pMT-V5-HisB-OXA1 (*Drosophila melanogaster*)-Apex2-Flag vector using a calcium phosphate transfection kit (Invitrogen), and protein expression was induced by $CuSO_4$. The cells were harvested 2–3 d postinduction, fixed with 2% glutaraldehyde, and subjected to the Apex2 staining procedure described above.

Western blot

Fly thoraxes were homogenized with a Dounce tissue grinder in RIPA buffer containing protease inhibitors (cOmplete; Roche). Cellular debris was removed by centrifugation at 14,000 × *g* for 20 min, 4°C. The supernatants were collected, and the protein concentrations were determined by Pierce protein assay (Pierce 660 nm Protein Assay Reagent; Thermo Scientific). Protein was loaded at 20 µg/well for SDS–PAGE and Western blot analysis.

The antibodies used in this study were as follows: mouse anti-ATP5A (1:50,000, abcam ab14748), mouse anti-cyto c (1:10,000, abcam ab13575), mouse anti-PDHA1 (1:1000, abcam ab110334), or rabbit anti-SOD2 (1:10,000, abcam ab13534), and rabbit anti-alpha tubulin (1:10,000, abcam ab18251), mouse anti-Flag M2 (1µg/ml, Sigma F3165), anti-mouse immunoglobulin G (IgG)-HRP (1:2000, Invitrogen 62-6520), or anti-rabbit IgG-HRP (1:5000, abcam ab97051). For quantification, the densiometric signal of individual proteins was normalized to that of α-tubulin. The ratios were then normalized to those from week 4 WT flies. Quantitative results in Figure 1e were generated from three independent samplings and Western blot analyses.

COX activity colorimetric assay

About 20 flies were anesthetized on ice. The thoraxes were dissected and homogenized in 200 µl ice-cold isolation buffer (320 mM sucrose, 10 mM EDTA, and 10 mM Tris-HCl, pH 7.3) using a Dounce tissue grinder. Cellular debris was removed by centrifugation at 600 × *g* for 5 min, 4°C. Mitochondria were harvested by centrifugation at 14,000 × *g* for 20 min, 4°C. Pellets containing mitochondria were resuspended in 100 µl enzyme dilution buffer (200 mM sucrose, 10 mM Tris-HCl, pH 7.0). The protein concentrations were determined by Pierce protein assay (Pierce 660 nm Protein Assay Reagent; Thermo Scientific).

The assay procedure was modified from the instructions for the COX colorimetric kit (BioVision K287). First, 1 ml of 0.5 mM cyt c was reduced by adding 5 µl 0.5 M dithiothreitol for 15 min at room temperature. For each reaction, 20 µl of reduced cyt c was diluted with 100 µl assay buffer (120 mM KCl, 10 mM Tris-HCl, pH 7.0) and 2 µg mitochondrial extract was added. COX activity was determined by the decrease of absorbance at 550 nm for 10 min, measured with a multiwell spectrophotometer. The readings were normalized to those for week 4 WT flies.

ACKNOWLEDGMENTS

We thank the EM facility of the Biomedical Sciences (AS-CFII-108-119) and the Academia Sinica Cryo-EM Center (AS-CFII-108-110), Academia Sinica, Taiwan. We thank Ya-Hui Chou for the helpful discussion on *Drosophila* genetics. We are thankful for the funding support from Academia Sinica AS-105-TP-B04 and MOST 105-2628-B-001-004-MY3.

REFERENCES

Agrell I (1953). The aerobic and anaerobic utilization of metabolic energy during insect metamorphosis. Acta Physiol Scand 28, 306–335.
Barbot M, Meinecke M (2016). Reconstitutions of mitochondrial inner membrane remodeling. J Struct Biol 196, 20–28.
Bonifacino JS, Glick BS (2004). The mechanisms of vesicle budding and fusion. Cell 116, 153–166.
Bonnefoy N, Fiumera HL, Dujardin G, Fox TD (2009). Roles of Oxa1-related inner-membrane translocases in assembly of respiratory chain complexes. Biochim Biophys Acta 1793, 60–70.
Cogliati S, Frezza C, Soriano ME, Varanita T, Quintana-Cabrera R, Corrado M, Cipolat S, Costa V, Casarin A, Gomes LC, *et al*. (2013). Mitochondrial cristae shape determines respiratory chain supercomplexes assembly and respiratory efficiency. Cell 155, 160–171.
Cogliati S, Enriquez JA, Scorrano L (2016). Mitochondrial cristae: where beauty meets functionality. Trends Biochem Sci 41, 261–273.
Davies KM, Strauss M, Daum B, Kief JH, Osiewacz HD, Rycovska A, Zickermann V, Kuhlbrandt W (2011). Macromolecular organization of ATP synthase and complex I in whole mitochondria. Proc Natl Acad Sci USA 108, 14121–14126.
Frezza C, Cipolat S, Martins de Brito O, Micaroni M, Beznoussenko GV, Rudka T, Bartoli D, Polishuck RS, Danial NN, De Strooper B, Scorrano L (2006). OPA1 controls apoptotic cristae remodeling independently from mitochondrial fusion. Cell 126, 177–189.
Gilkerson RW, Selker JM, Capaldi RA (2003). The cristal membrane of mitochondria is the principal site of oxidative phosphorylation. FEBS Lett 546, 355–358.
Gold VA, Chroscicki P, Bragoszewski P, Chacinska A (2017). Visualization of cytosolic ribosomes on the surface of mitochondria by electron cryo-tomography. EMBO Rep 18, 1786–1800.
Harner ME, Unger AK, Geerts WJ, Mari M, Izawa T, Stenger M, Geimer S, Reggiori F, Westermann B, Neupert W (2016). An evidence based hypothesis on the existence of two pathways of mitochondrial crista formation. Elife 5, e18853.
Hung V, Udeshi ND, Lam SS, Loh KH, Cox KJ, Pedram K, Carr SA, Ting AY (2016). Spatially resolved proteomic mapping in living cells with the engineered peroxidase APEX2. Nat Protoc 11, 456–475.
Huynen MA, Muhlmeister M, Gotthardt K, Guerrero-Castillo S, Brandt U (2016). Evolution and structural organization of the mitochondrial contact site (MICOS) complex and the mitochondrial intermembrane space bridging (MIB) complex. Biochim Biophys Acta 1863, 91–101.
Jayashankar V, Mueller IA, Rafelski SM (2016). Shaping the multi-scale architecture of mitochondria. Curr Opin Cell Biol 38, 45–51.
Jiang YF, Lin HL, Fu CY (2017a). 3D mitochondrial ultrastructure of Drosophila indirect flight muscle revealed by serial-section electron tomography. J Vis Exp 2017, doi: 10.3791/56567.
Jiang YF, Lin SS, Chen JM, Tsai HZ, Hsieh TS, Fu CY (2017b). Electron tomographic analysis reveals ultrastructural features of mitochondrial cristae architecture which reflect energetic state and aging. Sci Rep 7, 45474.
Keil M, Bareth B, Woellhaf MW, Peleh V, Prestele M, Rehling P, Herrmann JM (2012). Oxa1-ribosome complexes coordinate the assembly of cytochrome C oxidase in mitochondria. J Biol Chem 287, 34484–34493.
Lucic V, Forster F, Baumeister W (2005). Structural studies by electron tomography: from cells to molecules. Annu Rev Biochem 74, 833–865.
MacVicar T, Langer T (2016). OPA1 processing in cell death and disease - the long and short of it. J Cell Sci 129, 2297–2306.
Mannella CA (2006). Structure and dynamics of the mitochondrial inner membrane cristae. Biochim Biophys Acta 1763, 542–548.
Martell JD, Deerinck TJ, Sancak Y, Poulos TL, Mootha VK, Sosinsky GE, Ellisman MH, Ting AY (2012). Engineered ascorbate peroxidase as a genetically encoded reporter for electron microscopy. Nat Biotechnol 30, 1143–1148.
Pfeffer S, Woellhaf MW, Herrmann JM, Forster F (2015). Organization of the mitochondrial translation machinery studied in situ by cryoelectron tomography. Nat Commun 6, 6019.
Quintana-Cabrera R, Mehrotra A, Rigoni G, Soriano ME (2018). Who and how in the regulation of mitochondrial cristae shape and function. Biochem Biophys Res Commun 500, 94–101.
Rampelt H, Zerbes RM, van der Laan M, Pfanner N (2017). Role of the mitochondrial contact site and cristae organizing system in membrane architecture and dynamics. Biochim Biophys Acta 1864, 737–746.
Schorr S, van der Laan M (2018). Integrative functions of the mitochondrial contact site and cristae organizing system. Semin Cell Dev Biol 76, 191–200.

Scorrano L, Ashiya M, Buttle K, Weiler S, Oakes SA, Mannella CA, Korsmeyer SJ (2002). A distinct pathway remodels mitochondrial cristae and mobilizes cytochrome c during apoptosis. Dev Cell 2, 55–67.
Seligman AM, Karnovsky MJ, Wasserkrug HL, Hanker JS (1968). Nondroplet ultrastructural demonstration of cytochrome oxidase activity with a polymerizing osmiophilic reagent, diaminobenzidine (DAB). J Cell Biol 38, 1–14.
Soto IC, Fontanesi F, Liu J, Barrientos A (2012). Biogenesis and assembly of eukaryotic cytochrome c oxidase catalytic core. Biochim Biophys Acta 1817, 883–897.
Stoldt S, Wenzel D, Hildenbeutel M, Wurm CA, Herrmann JM, Jakobs S (2012). The inner-mitochondrial distribution of Oxa1 depends on the growth conditions and on the availability of substrates. Mol Biol Cell 23, 2292–2301.
Strauss M, Hofhaus G, Schroder RR, Kuhlbrandt W (2008). Dimer ribbons of ATP synthase shape the inner mitochondrial membrane. EMBO J 27, 1154–1160.
Suloway C, Shi J, Cheng A, Pulokas J, Carragher B, Potter CS, Zheng SQ, Agard DA, Jensen GJ (2009). Fully automated, sequential tilt-series acquisition with Leginon. J Struct Biol 167, 11–18.
Tennessen JM, Baker KD, Lam G, Evans J, Thummel CS (2011). The Drosophila estrogen-related receptor directs a metabolic switch that supports developmental growth. Cell Metab 13, 139–148.
Varanita T, Soriano ME, Romanello V, Zaglia T, Quintana-Cabrera R, Semenzato M, Menabo R, Costa V, Civiletto G, Pesce P, *et al*. (2015). The OPA1-dependent mitochondrial cristae remodeling pathway controls atrophic, apoptotic, and ischemic tissue damage. Cell Metab 21, 834–844.
Wu M, Gu J, Guo R, Huang Y, Yang M (2016). Structure of mammalian respiratory supercomplex I1III2IV1. Cell 167, 1598–1609 e10.
Zick M, Rabl R, Reichert AS (2009). Cristae formation-linking ultrastructure and function of mitochondria. Biochim Biophys Acta 1793, 5–19.